Solid Freeform Fabrication 2024: Proceedings of the 35th Annual International Solid Freeform Fabrication Symposium – An Additive Manufacturing Conference
Reviewed Paper

Correlation of Surface Topography with Fatigue Life and Failure Location in Additively Manufactured AlSi10Mg via Computed Tomography

L. Englert*, V. Schulze* and S. J. Dietrich*

*Institute for Applied Materials – Materials Science and Engineering, Karlsruhe Institute of Technology (KIT), Karlsruhe, Germany

Abstract

The fabrication of AlSi10Mg components via PBF-LB results in the formation of porosity and a rough surface topography. Depending on the relative position to the inert gas flow, the geometry of the component and other factors, these features are also distributed inhomogeneously, which has an adverse effect on fatigue performance. Computed tomography enables the measurement of the entire component surface, making it possible to locate failure critical spots on component surfaces. In this work, surfaces of additively manufactured components are analyzed by a novel method using computed tomography. This allows the visualization of the variation in roughness and near-surface porosity, which in turn facilitates the identification of failure critical spots and their comparison to real failure spots. Furthermore, the location of the failure critical spot can be predicted in 50% of the cases, while a correlation with fatigue life is found for low stress amplitudes.

Introduction

Surfaces of components fabricated via PBF-LB usually exhibit a rough surface, with the size of the corresponding surface features spanning multiple orders of magnitude. Furthermore, since the surface contains undercut features it cannot be fully characterized through optical or tactile measurements. Moreover, in addition to the variance in surface quality stemming from different build angles, additively manufactured components feature significant inhomogeneities in areas nominally produced under the same conditions [1]. For example, the dependence on the position on the build plate, which leads to different conditions with regard to the protective gas flow and the recoater blade, was identified as the cause of the uneven surface quality, although there are other unknown influencing factors [2]. The roughness parameters are greatly influenced by individual features such as adhering spatter particles [3]. Due to the non-uniform distribution of these features on the surface, the roughness parameters show a strong dependence on the position of the measurement. Since only a full surface measurement can ensure the detection of these critical features, the probability of detecting these features must be statistically reflected in the measurements. Especially parameters like the maximum valley depth S_v and the maximum peak height S_p often depend on singular features of a surface and are therefore particularly dependent on the location and size of the measurement. Since the S_v parameter has been shown to correlate with fatigue life, it seems desirable to characterize this value over the entire surface [4,5].

In recent years, microcomputed tomography (μCT) has developed into an instrument for measuring such surfaces [6,7]. For example, Kerckhofs et al. extracted line profiles out of μCT data and compared the resulting arithmetic mean roughness P_a values to conventional measured

values [8]. The method was precise for rough surfaces and it was therefore applicable to lattice structures.

In particular, being able to measure a larger area of the surface helps to characterize the inhomogeneous PBF-LB surfaces. Thus, further methods were developed to characterize surfaces with areal measurements. For cylindrical structures, an "unrolling" of the surface was utilized by translating the µCT data to cylindrical coordinates [4,9,10]. Using the surface determination module of commercial software, triangulating the data, and removing invisible surfaces, Townsend et al. obtained a surface height distribution from µCT data. [11]. Comparison of data obtained by this or other similar methods with conventional data obtained by confocal microscopy or coherence scanning interferometry showed that surfaces can be adequately characterized if the features are properly resolved by µCT.

The fatigue strength of additively manufactured parts is largely dependent on the surface quality [12]. The S_v parameter, which characterizes the depth of the deepest pit in the measurement area, was identified to be important for the fatigue properties [4,5]. With µCT measurements, it is also possible to characterize surface pits, which are not directly measurable in line of sight measurements. Du Plessis and Beretta used a target/actual comparison of the µCT-measured surface and the CAD surface to identify surface pits in rectangular bending specimens with circular taper [13]. While some of the specimens failed at the edges, several specimens failed at the surface pits. Dastgerdi et al. extracted line profiles from cylindrical specimens from µCT data [14]. An effective $\sqrt{area}$ value was calculated from the R_v value and possible near surface pores to predict failure origin and fatigue life based on Murakami's approach [15]. Only profiles with a high R_z value were evaluated, which may influence the maximum R_v value found. Nevertheless, the failure origin could be predicted in some cases, although no quantification of correct predictions was presented.

In this work, the as-built surface of additively manufactured specimens is characterized by µCT. An analysis of the entire surface reveals not only the maximum value of the S_v parameter and the depth of open pores, but also the location of these critical spots. The locations predicted by the maximum surface parameters are then compared with the failure critical locations found in fatigue tests. A correlation of surface parameters with cycles to failure is investigated for different load levels.

Methods

The specimens were fabricated using gas atomized AlSi10Mg powder supplied by m4p GmbH. The chemical composition of the powder is shown in Table 1. The powder had a D10 of 21.0 µm, D50 of 35.3 µm and a D90 of 57.5 µm with a filling density of 1.5 g/cm^3.

Table 1: Chemical composition of the AlSi10Mg powder in wt.-%.

Al	Fe	Si	Mg	Mn	Ti	Zn	Cu	Pb	Sn	Ni
Bal.	0.14	9.8	0.31	<0.01	0.01	0.01	<0.01	<0.01	<0.01	<0.01

Additive manufacturing was carried out with the PBF-LB process using an ORLAS Creator RA from O.R. Lasertechnologie GmbH. The system is equipped with a 250 W Yb fiber laser and

a round build plate with a diameter of 110 mm. The layer height was set to 30 µm and the nominal laser spot diameter was set to 40 µm. The samples were produced at 225 W laser power, 1000 mm/s scan speed, 150 µm line spacing, two contour lines, and a linear hatching strategy without skywriting with a 67° rotation of the hatching between layers. Of the 32 specimens manufactured in a single build job, 14 specimens with a gage diameter of 6 mm were tested in uniaxial fatigue with a frequency of 25 Hz on an Instron testing machine. The remaining specimens are part of an ongoing study. The surface was left in the as-built state.

An YXLON Precision µCT cone beam CT was used to record the µCT measurements. An acceleration voltage of 165 kV, a target current of 0.06 mA on the reflection target and a resolution of 10.5 µm were used for the measurement. For each reconstruction, 1860 projections were acquired over a 360° rotation on a Perkin Elmer XRD1620 AN flat panel detector with 2048 × 2048 pixels and a pixel pitch of 0.2 mm.

The µCT data was analyzed using a software described in previous work [16]. The software uses the CAD data as a reference for roughness measurements. A sliding measurement window is defined around each mesh cell of the CAD mesh for which roughness parameters are calculated. The CAD mesh information is used to determine the measurement direction and to remove the nominal surface shape. Figure 1 shows a schematic of how the surface is extracted from µCT data. The highest point normal to the surface is extracted as the surface. Voxels, which are segmented as air and are below this identified surface, are labeled as open porosity (shown in red). Descriptive parameters are also calculated for this open porosity data. The algorithm is described in more detail in [16].

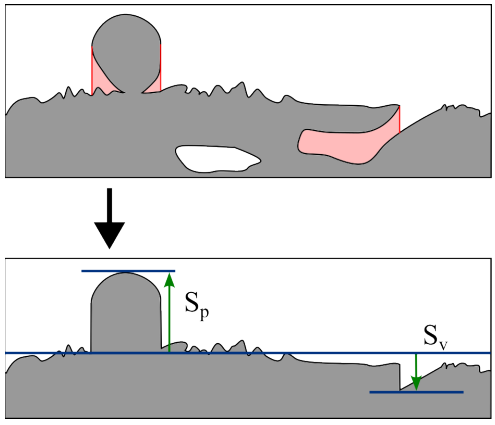

Figure 1: Schematic of extracted surface and definition of open porosity (red).

In the remainder of the work, especially two parameters will be relevant for evaluation of fatigue behavior. The maximum valley depth, S_v, will be evaluated since it was used for this purpose in related work. Similarly, the newly defined maximum depth of open pores parameter will be evaluated, since it also describes the depth of pits in the surface, but without being limited by the line of sight. For reference, Figure 1 shows a schematic representation of the measurement of the maximum peak height S_p and the maximum valley depth S_v.

Results and Discussion

Figure 2 shows the distribution of the maximum valley depth parameter S_v and of the depth of open pores value as box plots for each specimen. The mean values of the parameters exhibit only a slight variation between specimens, which is represented by colored bands in the graph. In contrast, the maximum values demonstrate a significant variation between specimens. For instance, the maximum S_v value varies between 162.9 µm and 362.5 µm, while the mean value only varies between 47 µm and 68 µm. The maximum depth of open pores varies between 220.5 µm and 441 µm.

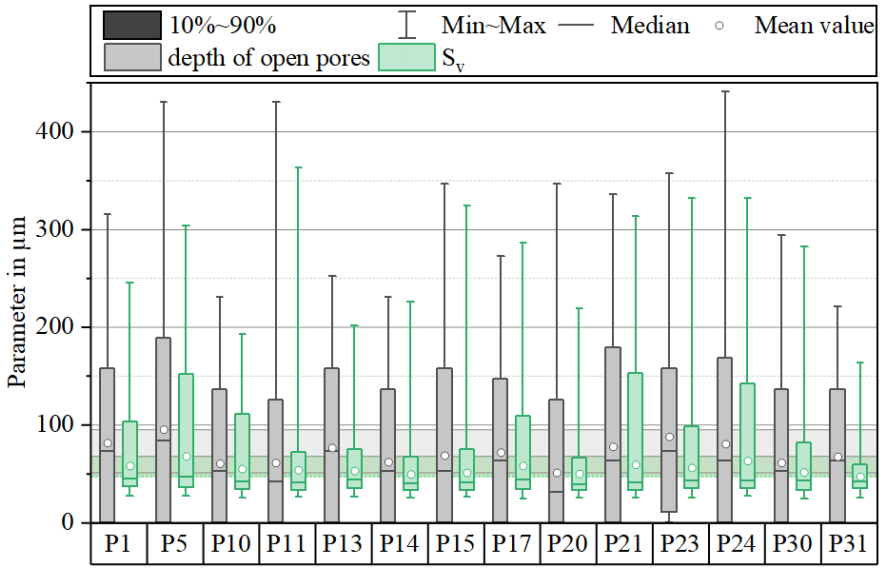

Figure 2: Distribution of the S_v value and the maximum depth of open pores in the analyzed samples. The ranges of mean values are shown as colored bands.

Figure 3 shows the spatial distribution of surface parameters on specimen P20. Figure 3a) and b) depict the distribution of the peak height value S_p on two adjacent sides of the specimen, while subfigure d) and e) show the valley depth value S_v on the respective sides. Subfigure f) depicts the distribution of the arithmetic mean height S_a. While the spatial variation of S_a is relatively continuous, the variation of S_p and S_v values is discontinuous. High values of S_p and S_v are located in distinct regions of approximately the same size as the measurement window. The values are calculated from the maximum and minimum height values, respectively, and thus exhibit a high or low value depending on whether a feature possessing a great height or depth is contained within a certain measurement window. Due to the different relative orientation of the surface to the recoater and the inert gas stream, the frequency of regions with high values is different on the two sides. Most high valued regions correspond to adhering spatter particles. When comparing the distributions of the two adjacent sides of the S_v value, there are smaller differences within the specimen visible. Figure 3c) shows the spatial distribution of the depth of open pores. Some of the regions with high values correspond to regions where the S_p value is also high. This is caused by air voxels identified below spatter particles, which count as open porosity. In contrast, the region with highest depth of open pores corresponds to a region with high S_v value. The pit at this location

contains air voxels, which are not measurable in line of sight, and therefore the depth of open pores is higher than the S_v value.

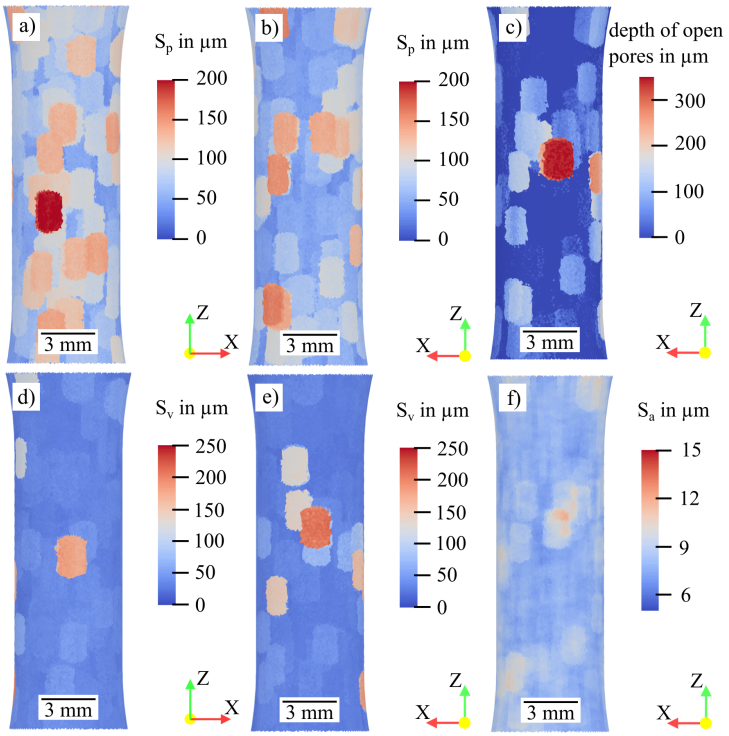

Figure 3: Visualization of surface parameter distributions in P20. S_p and S_v values are shown for two adjacent sides of the specimen.

Figure 4 shows the results of the fatigue tests. The relative scatter in fatigue life is similar for the specimens tested at 40 MPa and 100 MPa stress amplitude. At 100 MPa the fatigue life varied between 12700 and 21915 cycles and at 40 MPa load amplitude the fatigue life varied between 259580 and 446715 load cycles.

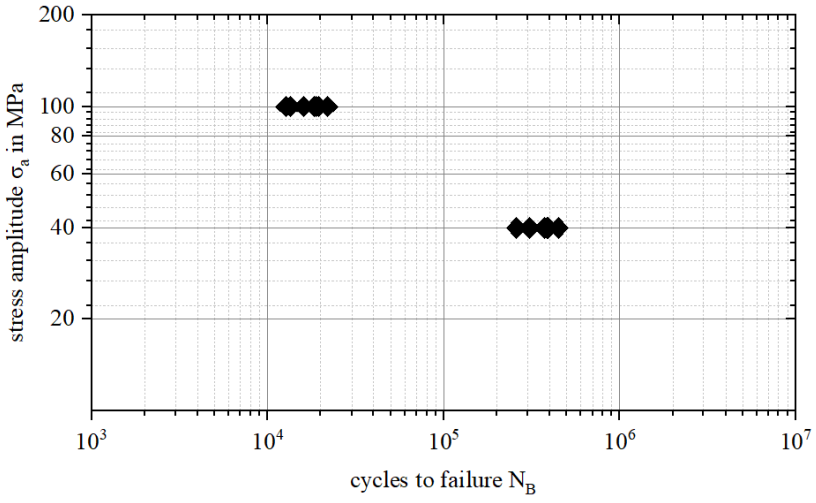

Figure 4: S-N curve of AlSi10Mg specimens with as-built surface.

At both load levels, all specimens failed at a surface open pore. Nonetheless, the specimens showed a different failure behavior at the two load levels. At 40 MPa, one to three sites were visible from which the fatigue crack initiated, while at 100 MPa, up to eight crack initiation sites were found in the fracture surface. A quantitative evaluation of this is shown in Figure 5. At the 100 MPa load level, some initiation sites were contained in the remaining fracture area.

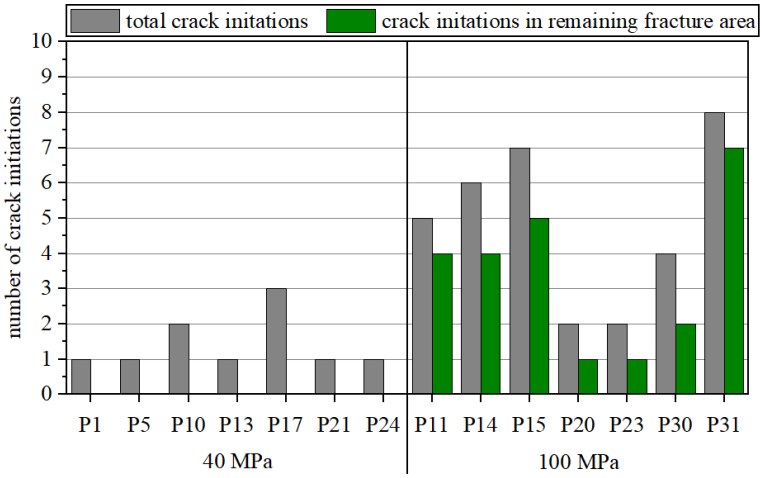

Figure 5: Count of crack initiations total and in remaining fracture area.

One of the objectives of this work is to correlate the fatigue life of a specimen with its surface quality. As a benchmark for the correlations to the surface quality parameters, the depth of the failure critical defect was measured using the fracture surface. Since these depths are measured only at the deepest flaw in the fracture area where the crack originated, the uncertainty corresponding to the criticality of the defects is eliminated. Therefore, these values can be used as a reference. In contrast, µCT analysis is performed on all pits in the surface and not just the failure critical ones. This means that the deepest defects do not automatically have to correspond to the failure-critical ones. Compared to concepts like Murakami's $\sqrt{area}$, no assumption is made about the defects acting like cracks, but rather it is investigated, under which circumstances defects size metrics correlate with fatigue life or failure location. Since the open pores do not possess a large aspect ratio, their $\sqrt{area}$ value is similar to their depth value.

Two depths were defined as sketched in Figure 6. The apparent depth t_A was measured taking line of sight into account, as a reference value for the S_v value. Pore depth t_B was measured without considering undercuts, comparable to the depth of open pores. Testing correlations between these parameters and fatigue life serves as a "best case" test, where only the depth of failure critical defects is considered. If no correlation between the fatigue life and t_A or t_B is found, it is not to be expected that one of the parameters from µCT characterization will correlate with fatigue life. This is due to the fact, that the maximum depths or S_v values from µCT may be measured at a pit that is not the failure critical location.

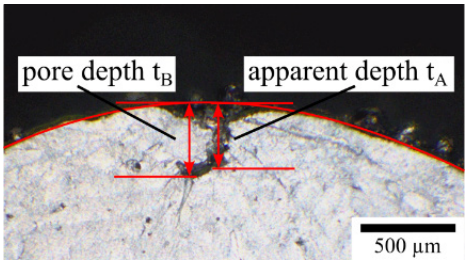

Figure 6: Measurement of depth of failure critical pore. Apparent depth t_A is measured in line of sight; pore depth t_B is measured without consideration of undercuts.

Figure 7 shows the investigated surface parameters on the ordinate and the fatigue life on the abscissa. The specimens tested with a stress amplitude of 40 MPa show a correlation of t_A (subfigure a)) respectively t_B (subfigure b)) with the cycles to failure, while the cycles to failure of the specimens tested with a stress amplitude of 100 MPa show no clear correlation. The values of apparent depth t_A and pore depth t_B differ only for two of the specimens tested with a stress amplitude of 40 MPa.

Subfigure c) shows the maximum S_v value, which was measured over the entire measurement length, plotted against the cycles to failure. As with the fracture surface measurement, the samples tested with a stress amplitude of 40 MPa show a correlation with the maximum S_v value, while the samples tested with a stress amplitude of 100 MPa show no clear correlation. The maximum depth of open pores measured by µCT plotted against the cycles to failure is shown in subfigure d). For the load level of 40 MPa, a correlation comparable to the S_v value can be seen. At the load level of 100 MPa, again no clear correlation can be seen, with one data point in particular deviating.

A linear regression between S_v and the cycles to failure of the specimens loaded with 40 MPa delivers a coefficient of determination of $R^2 = 0.76$. In comparison, the coefficient of determination between t_A and the cycles to failure is 0.68. The linear regression between the cycles to failure and the depth of open pores ($R^2 = 0.77$) respectively t_B ($R^2 = 0.69$) yields similar values. The slope of the linear regressions for the specimens loaded with 100 MPa did not differ significantly from zero, i.e. no correlation could be observed. This behavior might be explained by the fatigue life being dominated by the crack initiation at low stress amplitudes and by crack propagation at high load amplitudes [17]. Thus, the depth of surface pits only correlates with the cycles to crack initiation and not the crack propagation rate.

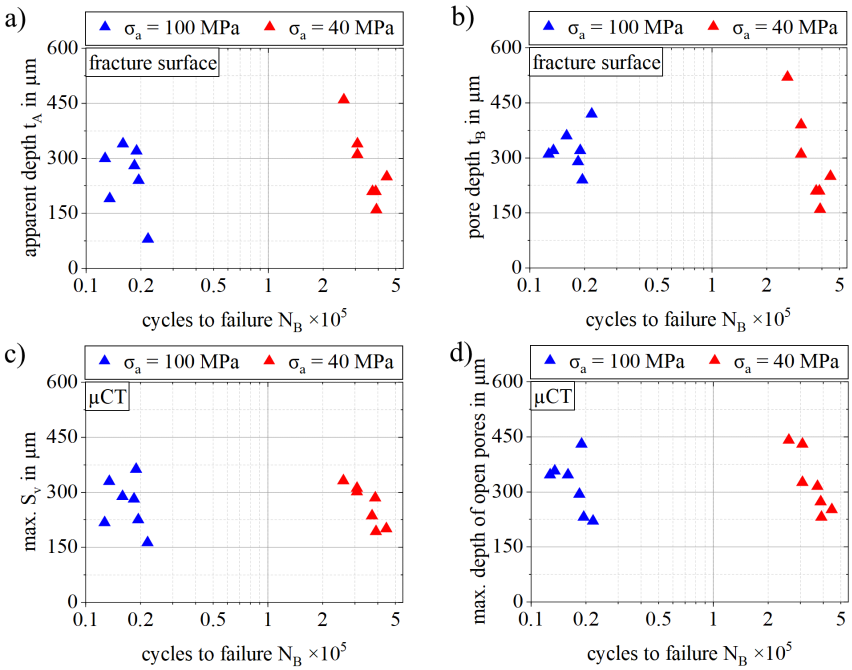

Figure 7: Correlations between number of cycles to failure and a): depth t_A; b) depth t_B; c) max. S_V value (µCT); d) max. depth of open pores (µCT)

Figure 8 illustrates the procedure used to compare the predicted failure critical location to the actual failure location. The location with the highest S_V value or open pore depth was used to predict the failure critical location. As mentioned above, high values of these parameters occur at locations of the size of the measurement window because these high values depend on whether the critical feature is included in the measurement window. Therefore, the midpoint of these locations corresponds to the predicted critical location.

The actual failure location was found by comparing the shape of the open pore from which the fatigue crack originated in the fracture surface to the µCT images and determining the location of this feature in the image. This is visualized as a black "x" in Figure 8.

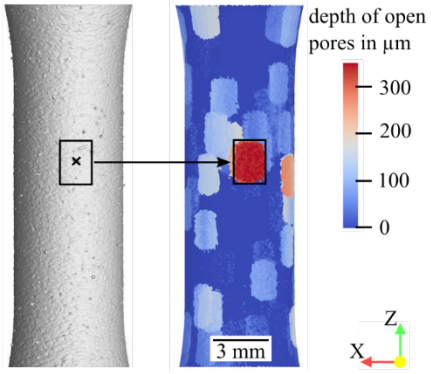

Figure 8: Example for consensus of real failure location (black x) and location of highest depth of open pores value (red).

To assess the prediction quality quantitatively, the ranking shown in Table 2 was derived from this comparison. If the actual failure critical location coincided with the predicted failure critical location, the location with the highest values, the ranking shows a "1". If the second-highest

ranked location corresponded to the actual failure location, the table shows a “2” etc. If the failure location was not found within the ten highest ranked spots, the table shows a “-“. Only for sample 31 no correct prediction was achieved, since the failure critical location was positioned slightly below the surface and therefore not segmented as open pore.

Table 2: Ranking of actual failure location among locations with high parameters. A '-' means the real failure location was not among the ten highest rated locations.

Load amplitude	Sample no.	Rank S_v	Rank max. depth of open pores
40 MPa	1	3	8
40 MPa	5	6	2
40 MPa	10	4	4
40 MPa	13	8	-
40 MPa	17	3	2
40 MPa	21	3	1
40 MPa	24	3	1
100 MPa	11	2	2
100 MPa	14	5	1
100 MPa	15	1	1
100 MPa	20	1	1
100 MPa	23	7	1
100 MPa	30	1	1
100 MPa	31	-	-

For 13 out of 14 specimens tested, the actual failure location was among the ten locations with highest S_v value or depth of open pores. With correct predictions in 50% of cases, the maximum depth of open pores predicted the actual failure location more often than the S_v value. In the three cases where the location of the highest S_v value was a correct prediction of the failure location, the maximum depth of open pores also correctly predicted the failure location. The prediction quality for the specimens loaded with 100 MPa was better than for the specimens loaded with 40 MPa, although no correlations were found when looking at the fatigue life. The nucleation of cracks depends on the magnitude of cyclic plastic slip at each potential failure location [17]. At higher load amplitudes microstructural obstacles can be overcome more easily, which means that cracks can be initiated even if the grain orientation is unfavorable, for example. Since the local microstructural conditions are not accessible in the µCT data, less dependence on these variables may explain the better prediction quality at higher load amplitudes.

Conclusions

In this study, the correlation between extremal values of surface quality and the fatigue life and failure location was investigated. For this purpose, the as-built surfaces of additively manufactured specimens were characterized by µCT. A correlation between fatigue life and the surface quality could be identified for a load amplitude of 40 MPa but not for the higher load amplitude of 100 MPa. Spatial variations of surface quality were linked to failure locations in fatigue testing. In 13 out of 14 cases, the prediction could narrow down the failure location to ten locations by one of the depth parameters. Future research will be dedicated to improving the prediction quality by incorporating pit curvatures in failure location prediction.

References

[1] S. Abolmaali, A. Vinel, J. Fox, J. Liu, D. Silva, Location and Orientation Dependency in Surface Roughness of Nickel Super Alloy 625 Parts: Statistical and Distributional Analysis, Solid Freeform Fabrication 2021: Proceedings of the 32nd Annual International Solid Freeform Fabrication Symposium (2021).

[2] R. Rothfelder, B. Baumgärtner, T. Hausotte, M. Schmidt, Surface layer porosity and surface quality in dependency of contour scanning strategy of Ti6Al4V parts, Procedia CIRP 111 (2022) 41–46. https://doi.org/10.1016/j.procir.2022.08.112.

[3] B. Whip, L. Sheridan, J. Gockel, The effect of primary processing parameters on surface roughness in laser powder bed additive manufacturing, Int J Adv Manuf Technol 103 (2019) 4411–4422. https://doi.org/10.1007/s00170-019-03716-z.

[4] J. Gockel, L. Sheridan, B. Koerper, B. Whip, The influence of additive manufacturing processing parameters on surface roughness and fatigue life, International Journal of Fatigue 124 (2019) 380–388. https://doi.org/10.1016/j.ijfatigue.2019.03.025.

[5] A. Yadollahi, M.J. Mahtabi, A. Khalili, H.R. Doude, J.C. Newman, Fatigue life prediction of additively manufactured material: Effects of surface roughness, defect size, and shape, Fatigue Fract Eng Mat Struct 41 (2018) 1602–1614. https://doi.org/10.1111/ffe.12799.

[6] A. Townsend, N. Senin, L. Blunt, R.K. Leach, J.S. Taylor, Surface texture metrology for metal additive manufacturing: a review, Precision Engineering 46 (2016) 34–47. https://doi.org/10.1016/j.precisioneng.2016.06.001.

[7] R.K. Leach, D. Bourell, S. Carmignato, A. Donmez, N. Senin, W. Dewulf, Geometrical metrology for metal additive manufacturing, CIRP Annals 68 (2019) 677–700. https://doi.org/10.1016/j.cirp.2019.05.004.

[8] G. Kerckhofs, G. Pyka, M. Moesen, S. Van Bael, J. Schrooten, M. Wevers, High-Resolution Microfocus X-Ray Computed Tomography for 3D Surface Roughness Measurements of Additive Manufactured Porous Materials, Adv Eng Mater 15 (2013) 153–158. https://doi.org/10.1002/adem.201200156.

[9] T. Persenot, A. Burr, R. Dendievel, J.-Y. Buffière, E. Maire, J. Lachambre, G. Martin, Fatigue performances of chemically etched thin struts built by selective electron beam melting: Experiments and predictions, Materialia 9 (2020) 100589. https://doi.org/10.1016/j.mtla.2020.100589.

[10] T. Fritsch, L. Farahbod-Sternahl, I. Serrano-Muñoz, F. Léonard, C. Haberland, G. Bruno, 3D Computed Tomography Quantifies the Dependence of Bulk Porosity, Surface Roughness, and Re-Entrant Features on Build Angle in Additively Manufactured IN625 Lattice Struts, Adv Eng Mater 24 (2022) 2100689. https://doi.org/10.1002/adem.202100689.

[11] A. Townsend, R. Racasan, R. Leach, N. Senin, A. Thompson, A. Ramsey, D. Bate, P. Woolliams, S. Brown, L. Blunt, An interlaboratory comparison of X-ray computed tomography measurement for texture and dimensional characterisation of additively manufactured parts, Additive Manufacturing 23 (2018) 422–432. https://doi.org/10.1016/j.addma.2018.08.013.

[12] N. Sanaei, A. Fatemi, Defects in additive manufactured metals and their effect on fatigue performance: A state-of-the-art review, Progress in Materials Science 117 (2021) 100724. https://doi.org/10.1016/j.pmatsci.2020.100724.

[13] A. Du Plessis, S. Beretta, Killer notches: The effect of as-built surface roughness on fatigue failure in AlSi10Mg produced by laser powder bed fusion, Additive Manufacturing 35 (2020) 101424. https://doi.org/10.1016/j.addma.2020.101424.

[14] J.N. Dastgerdi, H. Remes, O. Jaberi, Influence of internal and surface defects on the fatigue performance of additively manufactured stainless steel 316L, International Journal of Fatigue (2022).
[15] Y. Murakami, Metal Fatigue: Effects of Small Defects and Nonmetallic Inclusions, 2nd ed., Academic Press an imprint of Elsevier, Amsterdam, Niederlande, 2019.
[16] L. Englert, V. Schulze, S. Dietrich, Generalised and Automated Method for Surface Analysis of Roughness and Subsurface Porosity using Micro-Computed Tomography, NDT and E International (2023).
[17] J. Schijve, Fatigue of Structures and Materials, 2nd ed., Springer, Dordrecht, Niederlande, 2009.